Immobilization of polyoxometalate hybrid catalysts onto mesoporous silica supports using phenylene diisothiocyanate as a cross-linking agent

Ourania Makrygenni, Dalil Brouri, Anna Proust, Franck Launay, Richard Villanneau

Contents lists available at ScienceDirect

Microporous and Mesoporous Materials

journal homepage: www.elsevier.com

Immobilization of polyoxometalate hybrid catalysts onto mesoporous silica supports using phenylene diisothiocyanate as a cross-linking agent

Ourania Makrygenni[a], Dalil Brouri[b], Anna Proust[a], Franck Launay[b, **], Richard Villanneau[a, *]

[a] Sorbonne Université, CNRS UMR 8232, Institut Parisien de Chimie Moléculaire, Campus Pierre et Marie Curie, 4 Place Jussieu, F-75005, Paris, France
[b] Sorbonne Université, CNRS UMR 7197, Laboratoire de Réactivité de Surface, LRS, Campus Pierre et Marie Curie, F-75005, Paris, France

ARTICLE INFO

Keywords:
Polyoxometalate hybrids
Functionalized mesoporous silica materials
Epoxidation catalysis
Anchored homogeneous catalysts

ABSTRACT

The hybrid derivative of heteropolytungstate bearing two aniline groups, namely $(^nBu_4N)_3[NaHPW_9O_{34}\{As(O)C_6H_4NH_2\}_2]$, was post-functionalized in the presence of 1,4-phenylene diisothiocyanate (PDITC). The resulting molecular moiety was characterized by IR, ^1H and ^{31}P NMR spectroscopy. In a second step, this post-functionalized hybrid of polyoxometalate was covalently grafted onto the surface of an amino-functionalized SBA-15 silica by means of the formation of thiourea bonds. This simple and efficient strategy of immobilization did not require the use of a coupling agent and was performed in mild reaction conditions. Various physicochemical techniques (^{13}C and ^{31}P CP—MAS NMR spectroscopies, XPS, XRF, HR-TEM microscopy and N_2 sorption) contributed to the full characterization of the supported catalyst. In addition HR-TEM was found to be an essential technique for the identification of the polyoxometalate units inside the pores of SBA-15. Finally, the catalytic performances of the supported polyoxometalates were evaluated in the epoxidation of cyclooctene with aqueous H_2O_2 in acetonitrile at 50 °C.

1. Introduction

During the past decades, continuous attention was given to polyoxometalates-based catalytic materials because of their numerous advantages in catalysis [1]. In the first place, polyoxometalates (POMs) may exhibit strong Bronsted-type acidity in their heteropolyacid form, making them suitable for various acidic reactions [2], but some POMs that possess basic properties can also be used in base-catalytic reactions [3]. In addition, other catalytic processes such as organic group transfer reactions (carbene transfer [4], aziridination [5] and cyclopropanation [6] reactions) have been more rarely illustrated. Most applications of POMs in catalysis refer however to oxidation reactions. Indeed, it is well known that POMs (including transition-metal derivatives) have fast and reversible multi-electron redox processes, and that they are able to react with H_2O_2 to form peroxo species. This characteristic makes them generally efficient candidate catalysts for the oxidation of alkanes, aromatics, olefins, alcohol, and so on [7]. Equally important, the chemical properties of POMs, their acid-base strength, redox potentials and solubility in aqueous or organic media, can be easily tuned on purpose by smoothly varying their composition and structure [8]. Moreover, compared with other common coordination and/or organometallic complexes, POMs are thermally and oxidatively stable toward oxygen donors. Nevertheless, POMs are usually soluble in many polar solvents, causing difficulties in the recovery, separation, and recycling of the catalysts. This potentially affects their use in systems that require environmentally friendly efficient transformations and sustainable development. As a result, it is necessary to develop easily recoverable and recyclable POMs-based catalysts for practical application in industry. To achieve this, heterogeneous catalysts are preferred because of their advantages on facile catalyst/product separation [9,10]. Some of our recent works dealt with developing covalent grafting procedures of hybrid derivatives of POMs [11] bearing carboxylic acid groups onto silica supports, previously functionalized with aminopropyl groups (using APTES). Indeed, we initially anchored POM hybrids onto various mesoporous silica oxides (SBA-15 and Mesocellular Foam) [12]. This strategy was recently successfully transposed to the functionalization of core-shell magnetic nanoparticles, in which the cores consisted of maghemite nanocrystals embedded within a silica shell [13]. This shell was then surrounded by aminopropyl functions and polyethyleneglycol (PEG) chains for their stabilization. In both

* Corresponding author. Sorbonne Université, CNRS UMR 8232, Institut Parisien de Chimie Moléculaire, Campus Pierre et Marie Curie, 4 Place Jussieu, F-75005, Paris, France.
** Corresponding author.
Email address: richard.villanneau@sorbonne-universite.fr (R. Villanneau)

https://doi.org/10.1016/j.micromeso.2018.11.036
Received 7 September 2018; Received in revised form 10 November 2018; Accepted 27 November 2018
Available online xxx
1387-1811/

cases (mesoporous supports and nanoparticles) the immobilization of the POM required the use of a coupling agent (isobutylchloroformiate) and a base (triethylamine). This strategy allowed an excellent nanostructuration of the POMs shell at the surface of both types of silica support, as determined by High-Resolution Transmission Electronic Microscopy. We equally demonstrated that the covalent anchorage of POMs increased the link strength between POMs and supports. Limitations of this approach lied however on the low control of the quantity of POMs grafted onto the surface of the oxides, which hardly corresponded to the amount of POMs engaged during the catalysts preparation (see Table 1).

Another strategy was explored in the present work and consisted of anchoring functionalized POMs through the use of a cross-linker between POM hybrids and an amino-functionalized silica. Cross-linkers are commonly used in biological applications, especially for the grafting of proteins on surfaces for the generation of biochips. Generally, the most common encountered cross-linkers in the literature carry two similar functions, such as dialdehydes [14] or diisothiocyanate [15]. These derivatives are indeed able to form specific covalent bonds with a surface at one end and with the desired molecule at the other end. Representative examples are often based on the activation of glass slides [16], amino-silica surfaces [17,18], magnetic core-shell nanoparticles [19], silica nanoparticles [20], or even silanized surfaces [21] by a cross-linker such as 1,4-phenylene diisothiocyanate (PDITC), being used in the present work. By contrast, examples of bulk mesoporous materials (such as SBA-15 used in the present work) post-functionalized using PDIT are scarce in the literature [22].

An attractive feature of this approach lays on the fact that the spectroscopic fingerprint of the cross-linkers in the final materials provides a useful tool of characterization for the link between both partners. Several issues were addressed in this work: i) the reaction of the aminophenylarsonyle derivative of POM namely $(^{n-}Bu_4N)_3[NaHPW_9O_{34}\{As(O)C_6H_4\text{-}p\text{-}NH_2\}_2]$ (compound **1**, Fig. 1) with PDITC, ii) the covalent immobilization of the new hybrid derivative onto the surface of an amino-functionalized SBA-15 (for short {NH_2}—SBA-15), including the characterization of the covalent link between both partners and iii) the evaluation of the catalytic performance of the anchored catalysts within the frame of the epoxidation of cyclooctene as a model reaction.

Table 1
Percentage of W and As, and POMs loading for POM grafted materials by XRF spectroscopy. * based on $[NaHPW_9O_{34}\{As(O)C_6H_4—NH—C(S)—NH—C_6H_4NCS)\}_2]^{3-}$ anions (anion M_w = 2914 g mol^{-1}).

Elements	Weight content (%)	POMs loading (wt.%)*	POMs content (mmol.g^{-1})
W	9.65	17.0	0.058
As	0.84	16.3	0.056

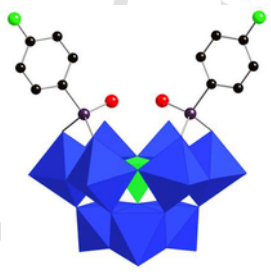

Fig. 1. Crystal Maker representation of the anion of $(^{n-}Bu_4N)_3[NaHPW_9O_{34}\{As(O)C_6H_4\text{-}p\text{-}NH_2\}_2]$ (**1**). W and P polyhedra are respectively depicted in blue and green; C, O, As and N atoms are represented as black, red, prune and green balls. (For interpretation of the references to colour in this figure legend, the reader is referred to the Web version of this article.)

2. Materials and methods

Solvents and other reagents were obtained from commercial sources and used as received. Compound **1** was prepared as previously described [23]. IR spectra were obtained from KBr pellets on a Jasco FT/IR-4100 spectrometer or by Attenuated Total Reflection Infra-Red spectroscopy, using Tensor R27 FTIR equipped with a ZnSe crystal with resolution better than 1 cm^{-1}. The ^{1}H and {^{1}H} ^{31}P NMR solution spectra were recorded in 5 mm o.d. tubes on a Bruker Avance II 300 spectrometer equipped with a QNP probehead. ^{13}C CP MAS NMR spectra were recorded at 125.77 MHz on a Bruker AVANCE III 500 spectrometer (11.7 T) with a 4 mm Bruker probe and at a spinning frequency of 10 kHz (Recycle delay = 5 s, contact time = 10 ms). ^{31}P MAS NMR spectra were recorded at 283.31 MHz on a Bruker AVANCE III 700 spectrometer (16.4 T) equipped with 2.5 mm Bruker probe and at a spinning frequency of 30 kHz. Chemical shifts were referenced to tetramethylsilane (TMS) for ^{13}C and to 85% aqueous H_3PO_4 for ^{31}P. X-ray photoelectron spectroscopy (XPS) spectra were performed on an Omicron (ESCA+) spectrometer, using an Al Kα X-ray source (1486.6 eV) equipped with a flood gun. HR-TEM analyses were realized on a microscope operating at 200 kV with a resolution of 0.18 nm (JEOL JEM 2011 UHR) equipped with an XEDS system (PGT IMIX-PC). Samples were deposited on Cu grid covered with an amorphous carbon film. X-Ray Fluorescence analyses were conducted with an energy dispersive spectrometer XEPOS with Turboquant powder software. N_2 sorption analyses of the pre-treated materials (100 °C) were obtained at −196 °C using an ASAP-2020 Micromeritics apparatus.

2.1. Functionalization of 1 with 1,4-phenylene diisothiocyanate (PDITC): synthesis of $(^{n-}Bu_4N)_3[NaHPW_9O_{34}\{As(O)C_6H_4\text{-}p\text{-}NH\text{-}C(S)—NH\text{-}p\text{-}C_6H_4NCS)\}_2]$ (2)

$(^{n}Bu_4N)_3[NaHPW_9O_{34}\{As(O)(C_6H_4\text{-}p\text{-}NH_2)\}_2]$ (1 g, 0.33 mmol) was introduced in a round flask and dissolved in 50 mL of acetonitrile. Then, PDITC (0.51 g, 2.65 mmol) was added to the solution and the mixture was left under stirring at RT for 7 days. Afterwards, the solution was left for partial evaporation in air for several days. A white precipitate of PDITC gradually appeared and was discarded by filtration (*ca.* 0.25 g). After one week, the residual solution was evaporated until dryness and the remaining yellow/orange powder was washed with several fractions (10 mL) of ethanol and diethyl ether until no remaining PDITC was detected by ^{1}H NMR spectroscopy, yielding 1.05 g (93%) of compound **2**; RMN ^{31}P{^{1}H} [121.5 MHz, CD_3SOCD_3]: -12.23 ppm; ^{1}H NMR [300.13 MHz, CD_3SOCD_3]: 0.94 (t, 36H, CH_3CH$_2$CH$_2$CH$_2$N), 1.32 (24H, CH$_3$CH_2CH$_2$CH$_2$N), 1.58 (24H, CH$_3$CH$_2$CH_2CH$_2$N), 3.17 (24H, CH$_3$CH$_2$CH$_2$CH_2N), 7.41 (8H, multiplet, aromatic in meta of NH thiourea), 7.58 (8H, multiplet, aromatic in ortho of thiourea), 10.11 ppm (4H, s, —NH—C=S-); ^{1}H NMR [300.13 MHz, CD_3CN]: 1.00 (t, 36H, CH_3CH$_2$CH$_2$CH$_2$N), 1.41 (sext, 24H, CH$_3$CH_2CH$_2$CH$_2$N), 1.64 (m, 24H, CH$_3$CH$_2$CH_2CH$_2$N), 3.14 (m, 24H, CH$_3$CH$_2$CH$_2$CH_2N) 7.35–7.92 (20H, multiplets, aromatic + thiourea), IR (KBr, cm^{-1}): 369 (m), 488 (m), 510 (m), 730 (s), 806 (sh), 850 (vs), 938 (sh), 963 (s), 1027 (m), 1083 (s), 1245 (s), 1307 (s), 1503 (s), 1595 (m), 2874 (m), 2936 (sh), 2962 (s), 3039 (w), 3095 (w), 3325 (m).

2.2. Preparation of {NH_2}—SBA-15

The amino-functionalized SBA-15 (for short {NH_2}—SBA-15) was obtained in a two-steps procedure, by the functionalization of a pre-formed SBA-15 with 3-aminopropyltriethoxysilane, as described previously [24]. The general formula of {NH_2}—SBA-15 is $H_2N(CH_2)_3SiO_{1.5}/8SiO_2$.

2.3. Covalent binding of 2 with {NH_2}—SBA-15

Samples of **2** (0.280 g, 0.075 mmol) and {NH_2}—SBA-15 (0.165 g, 1.69 mmol g^{-1} of —NH_2 groups, corresponding to 0.279 mmol of -{NH_2} groups) were introduced in a round-bottom flask and dispersed in 20 mL of acetonitrile. The mixture was left for stirring at RT for several days. Then, the final material (**2**@{NH_2}—SBA-15) was filtered and washed with refluxing acetonitrile using a Soxhlet for 48 h.

2.4. Catalytic studies

In homogeneous conditions, experiments of cyclooctene epoxidation were performed in a 50 mL round-bottom flask equipped with a condenser and magnetic stirrer at room temperature or at 50 °C. The catalyst (24 μmol, corresponding respectively to 80 mg for **1** and 90 mg for **2**), 20 mL of acetonitrile, 0.78 mL of cyclooctene (6 mmol/250 eq.), 0.90 mL of decane (as an internal standard) and 0.60 mL of an aqueous solution (30%) of H_2O_2 (6 mmol/250 eq) were introduced successively in the flask. The resulting solutions were analyzed after 24 h by gas chromatography on a Delsi Nermag DN 200 GC apparatus equipped with a flame ionization detector and a Macherey-Nagel Optima-5 capillary column (length 30 m, internal diameter 0.32 mm, thickness 1 μm).

In heterogeneous conditions, experiments of cyclooctene epoxidation were performed in 5 mL flasks under stirring at 50 °C. The solid catalysts **2**@{NH_2}—SBA-15 (21 mg), corresponding to 1.2 μmol (1 eq.) of **2**, 1 mL of acetonitrile, 39 μL (300 μmol) of cyclooctene (250 eq.), 45 μL of decane, and 30 μL of H_2O_2 (30% in water, 300 μmol, 250 eq.) were introduced successively in the flask. The supernatant of the resulting suspension was analyzed after 24 h by gas chromatography as described above. Blank reactions have been also performed with the support {NH_2}—SBA-15 before the POMs-grafting step. No catalytic activity was found for these materials in the absence of the POMs.

3. Results and discussion

3.1. POMs functionalization and characterization

3.1.1. Synthesis of compound 2

The strategy used in this study dealt with the post-functionalization of compound **1** with PDITC prior to its grafting onto {NH_2}—SBA-15 (as described in Fig. 2). Indeed aniline functions are less nucleophilic than the propylamine groups grafted onto SBA-15. Furthermore, the characterization of the functionalized POM is easier to perform by using common characterization techniques of molecular compounds.

The experimental protocol for **2** was chosen in order to avoid the formation of POMs dimers by direct reaction of two equivalents of POMs with the two SCN— terminations of the cross linker at once. The reaction was thus carried out in (moderately) dilute solution and with a large excess of PDITC in acetonitrile. It is noteworthy that the formation of thiourea functions was monitored by ^{1}H NMR, and was found relatively slow at room temperature when reacting with aniline functions.[1] The crude product, which contained in majority the desired (^{n}–$Bu_4N)_3$[$NaHPW_9O_{34}${$As(O)C_6H_4$—NH—C(S)—NH—C_6H_4NCS}$_2$] (compound **2**), was obtained after a slow evaporation (one week) of the solvent. This partial evaporation is an important step for removing most of the remaining PDITC that is less soluble in acetonitrile. At this step, the presence of PDITC may be easily characterized by ^{1}H NMR spectroscopy (singlet at 7.51 ppm in CD_3SOCD_3, see SI Fig. S2). Careful

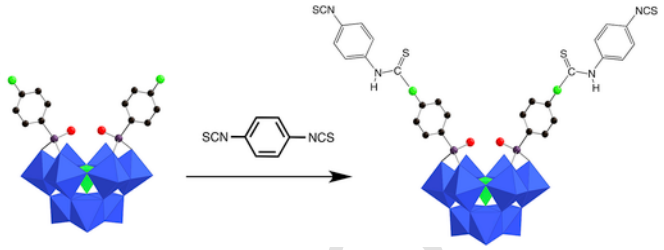

Fig. 2. Synthetic route for post-functionalization of (^{n}Bu$_4$N)$_3$[$NaHPW_9O_{34}${$As(O)C_6H_4$—NH_2}$_2$] (**1**) by PDITC leading to the formation of compound **2**.

washings with diethylether and ethanol allowed obtaining samples without PDITC.

3.1.2. Spectroscopic characterization of 2

Compound **2** was characterized by IR (Fig. 3), ^{1}H (Figs. S2 and S3) and ^{31}P NMR spectroscopy (Fig. S4). Comparison of the IR spectra of compounds **1** and **2** in the range 1100–700 cm^{-1} showed that the polyoxotungstate core was maintained during the post-functionalization reaction, since both spectra exhibited the same patterns in this region.

Furthermore, the $\nu_{as(NH)}$ (3365 cm^{-1}) and $\nu_{s(NH)}$ (3240 cm^{-1}) modes characteristic of the aniline {—NH_2} functions in **1** were replaced by a single broad band with a maximum at 3315 cm^{-1}, consistent with the formation of thiourea {—NH—CS—NH—} functions. The absence of the {NH_2} functions can also be disclosed by the disappearance of the in plane δ_{NH} at 1635 cm^{-1} in the spectrum of **1**. The presence of two supplementary bands in the spectrum of **2** in the range 1400–1200 cm^{-1} was also in accordance with the presence of thiourea functions. These two bands correspond respectively to the $\nu_{(C=S)}$ (1245 cm^{-1}) and to the equivalent of "amide III" (mainly $\nu_{(CN)}$ mode) at 1325 cm^{-1} and did not appear in the spectrum of PDITC (see Fig. S5). It is worth noting that the "amide II" band ($\delta_{(NH)}/\nu_{(CN)}$ mixed modes) cannot be distinguished here from the $\nu_{C=C(ar)}$ (1595 cm^{-1}) in the present spectrum. Furthermore, we observed two strong bands that are present in the spectrum of PDITC due to the presence of the remaining

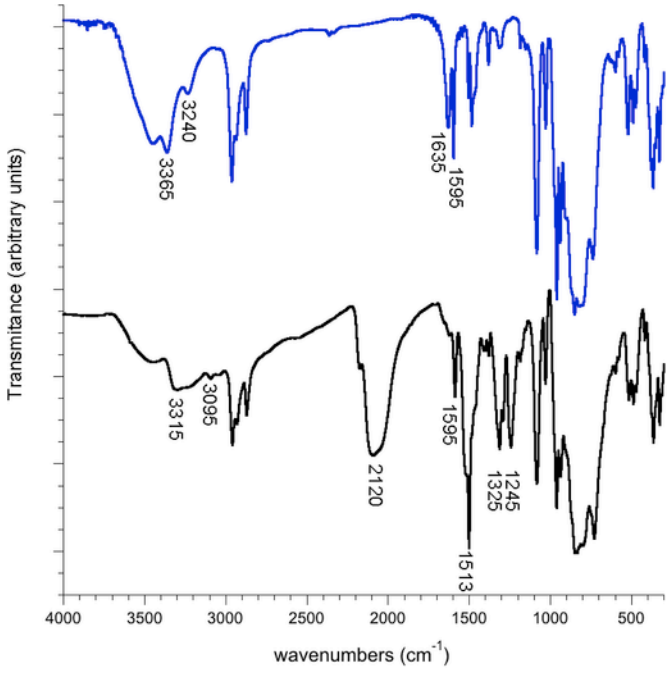

Fig. 3. IR spectra of compound **1** (blue) and **2** (black). (For interpretation of the references to colour in this figure legend, the reader is referred to the Web version of this article.)

[1] The formation of large amounts of unidentified side-on products was observed when the reaction was carried out at higher temperature.

—NCS terminations: a broad and highly intense band around 2120 cm^{-1} (attributed to the $\nu_{(N=C=S)}$ vibrations) and a sharp $\nu_{(C=N)}$ band at 1513 cm^{-1}. An enhancement of the $\nu_{(CHar)}$ at 3095 cm^{-1} was also observed in accordance with the introduction of supplementary aryl groups from grafted PDITC.

The ^1H NMR spectrum of **1** in CD_3SOCD_3 is characterized by the presence of two multiplets (8H, CH_{ar}) at 7.40 and 6.72 ppm and by a singlet (4H, —NH_2) at 6.01 ppm (see Fig. S1). The ^1H NMR spectrum of **2** in CD_3SOCD_3 (Fig. S2) is characterized by the presence of a singlet at 10.11 ppm (4H, N*H*—C=S) and two multiplets at 7.58 (8H, CH_{ar}) and 7.41 ppm (8H, CH_{ar}), and by the disappearance of the peak at 6.02 ppm, attributed to —NH_2 functions in the spectrum of **1**. Furthermore, the integration of the signals of the three methylene and of the methyl groups of the ^{n}-Bu_4N^+ cations is in accordance with the presence of three tetrabutylammonium counterions.

It is worth noting that this spectrum is strongly dependent on the solvent. Indeed, when the spectrum is performed in CD_3CN (see Fig. S3) the profile of the bands is significantly different, since the CH_{ar} atoms are characterized by four separated doublets in the range 7.25–8.00 ppm, and by the modification of the chemical shift of the {N*H*—C=S} protons which cannot be distinguished from the aromatic protons in this solvent.

Finally, compound **2** was also studied by ^{31}P NMR spectroscopy (see SI Fig. S4). The spectrum of the complex was characterized by a single peak at −12.23 ppm in CD_3SOCD_3, close to that of the parent compound **1** (−12.37 ppm).

3.2. POMs grafting onto the {NH_2}-functionalized SBA-15 and characterization of the resulting materials

The post-functionalized compound **2** was then grafted onto {NH_2}—SBA-15. The synthesis was carried out by simple impregnation of {NH_2}—SBA-15 with a solution of **2** in acetonitrile at room temperature for one week. The optimal ratio **2**/{—NH_2} functions used for the grafting was fixed to *ca.* 1/4 in order to obtain materials with both still high specific surface and an important POMs loading. Using these conditions, the amount of POMs, quantified by XRF spectroscopy, was found at *ca.* 16.7% (calculated by taking the average of the percentage of POMs obtained respectively from the weight content of W and As), with an experimental W/As ratio of 4.68, in accordance with the theoretical ratio in the POM (expected 4.5). We also tried to incorporate more hybrid POMs with a second cycle of POMs grafting, using a similar protocol. The thus obtained material was also characterized by XRF, but in these conditions we found that the increase in POMs loading was not significant enough regarding the implementation of a second cycle of reaction and washing steps.

The pore properties of the materials were analyzed from their nitrogen adsorption-desorption isotherms and their Brunauer-Emmet-Teller (BET) surface areas; the results are shown in Fig. 4 and Table 2.

As shown in Fig. 4, the N_2 adsorption-desorption isotherms of the SBA-15 based materials exhibited characteristic type IV patterns, which indicated that all materials were constituted of mesoporous channels with rather uniform diameters. When compound **2** was grafted onto {NH_2}—SBA-15, the S_{BET} value and the mean pore diameter of the resulting material **2**@{NH_2}—SBA-15 were significantly lower than those of {NH_2}—SBA-15, showing that the grafting was successful. The final BET specific surface area obtained was 438 m^2/g, a value significantly higher than the one obtained in our previous work [25]. This was probably due to a lower POMs content in the present case (0.057 mmol g^{-1} *vs.* 0.10 mmol g^{-1} in that above mentioned study). It should be added that an increase of the surface concentration of the propylamine groups in {NH_2}—SBA-15 materials led to a significant decrease of the pores diameter/volume (as determined from their nitrogen adsorption/desorption isotherms) and consequently to a dramatic

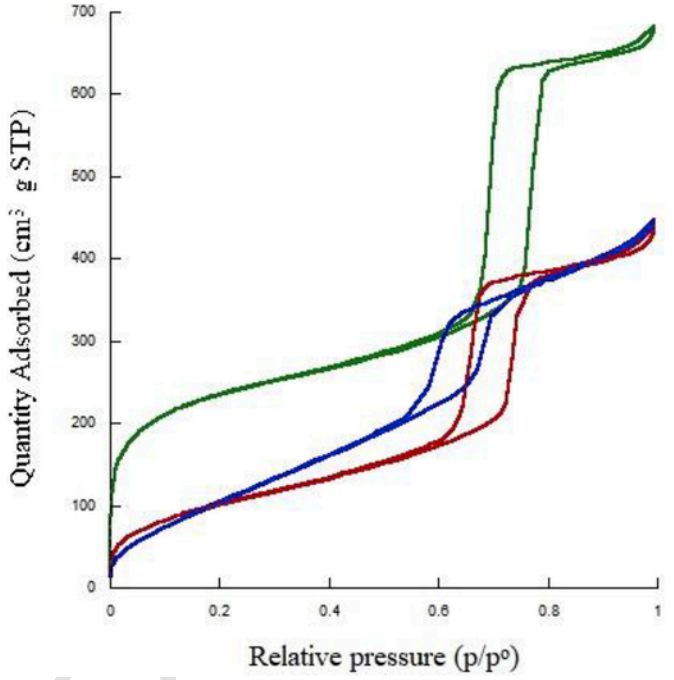

Fig. 4. Nitrogen adsorption-desorption isotherms of SBA-15 (green line), {NH_2}—SBA-15 (red line) and **2**@{NH_2}—SBA-15 (blue line). (For interpretation of the references to colour in this figure legend, the reader is referred to the Web version of this article.)

Table 2
Textural data of SBA-15, {NH_2}—SBA-15 and **2**@{NH_2}—SBA-15

	S_{BET} (m^2/g)	Pore vol. (cm^3/g)	Pore diameter (nm)
SBA-15	985	1.0	6.5
{NH_2}—SBA-15	595	0.69	5.8
2@{NH_2}—SBA-15	438	0.60	4.5

decrease of the POMs amount after the grafting steps [25]. The materials used in the present work thus correspond to the optimal compromise between the surface {NH_2}-concentration and the textural parameters.

The hybrid material, namely 2@{NH_2}—SBA-15, was then characterized by HR-TEM (Fig. 5), showing that the mesoporous network is clearly maintained (see also Fig. S6). This result highlights the importance of using mild conditions during the grafting step, since the intrinsic structure of the amino-functionalized SBA-15 is not affected by the grafting of **2**. In addition, POMs are clearly identified in the micrograph presented in Fig. 5 and are located inside the channels of the amino-functionalized SBA-15. The size of the black dots corresponds roughly to the diameter of an isolated POM (*ca.* 1 nm), indicating that the POMs introduced are not aggregated.

The examination of the local elemental composition of the samples was also achieved using X-Ray Energy-Dispersive Spectroscopy (XEDS). The W/As and W/S ratios found (respectively 3.73 and 3.22) are close to that expected (respectively 4.5 and 2.25).

The XPS spectrum of 2@{NH_2}—SBA-15 was also recorded. High-resolution W_{4f} and N_{1s} spectra are displayed respectively on Fig. 6. The W_{4f} peak was composed of a well-resolved spin-orbit doublet (35.6 and 37.7 eV for $W4f_{7/2}$ and $W4f_{5/2}$, respectively), typical of W^{VI} atoms on Keggin-type POMs [26,27]. The N_{1s} peak was composed by two unequivalent components. The less intense peak (402 eV) was assigned to ammonium ions (in the present case tetrabutylammonium and propylammonium resulting from partial protonation of propylamine groups of the SBA-15), while the peak at lower energy (399.9 eV) may be asso-

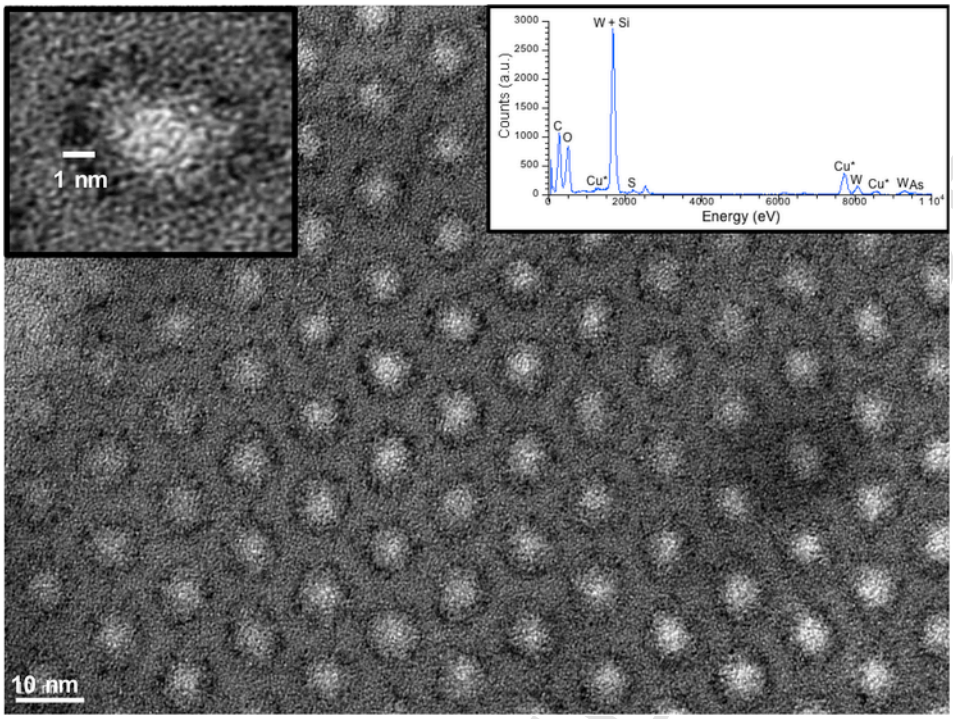

Fig. 5. HR-TEM micrograph (microtome cutting) of amino-functionalized SBA-15 decorated with **2** (**2**@{NH_2}—SBA-15). Insert: XEDS spectrum of the material. The peaks with an asterisk correspond to the Cu element contained in the grid support.

ciated to the propylamine functions covering the amino-functionalized SBA-15. It is noteworthy that the position of the peak attributed to the N atom of thiourea functions (expected at *ca.* 400 eV) [28] cannot be distinguished from that of propylamine functions. Finally, high-resolution C_{1s}, O_{1s} and Si_{2p} spectra were also recorded but they did not give any supplementary significant information.

The ^{13}C CP—MAS NMR spectrum of **2** was recorded in the solid state before grafting onto the {NH_2}—SBA-15 support (Fig. 7). It displayed four peaks with a chemical shift lower than 60 ppm attributed to the four carbon atoms of the tetrabutylammonium ions. In addition, three major peaks were also observed in the range 120–150 ppm. The most intense peak was attributed to the aromatic carbons (126 ppm). The carbon atom corresponding to the remaining isothiocyanate functions of **2** was located at around 138 ppm (137 ppm in solution in $CDCl_3$ for PDITC). Lastly, the peak at 179 ppm may be tentatively assigned to the carbon atom from the {NH—*C*(=S)—NH} thiourea function, as expected for such a group, by comparison with the spectrum of diphenylthiourea in solution [29].

The ^{13}C CP-MAS NMR spectrum of **2**@{NH_2}—SBA-15 was then recorded and presented Fig. 7 (bottom). This spectrum displayed three peaks with chemical shift values lower than 50 ppm assigned to the aminopropyl functions, as the major components in this area. The signals attributed to the aromatic carbon atoms were still present but somewhat broad (maximum at $\delta = 131$ ppm). A shoulder at 136 ppm was also observed and it was attributed to residual –NCS functions. It is noteworthy that not all the —NCS functions of **2** were grafted at the surface of the {NH_2}—SBA-15 support, probably because the distance between the isothiocyanate functions in **2** does not match with the distribution of the —NH_2 groups at the surface. In parallel, a peak at $\delta = 180$ ppm was observed, which corresponds to the carbon atom of the thiourea functions. The relative intensity of this peak seems particularly important compared to the spectrum **2**. In conclusion, it is tempting to correlate the decrease of the peak at $\delta = 136$ ppm in parallel with the apparent increasing intensity of the peak at $\delta = 180$ ppm to the formation of additional thiourea functions in the supported materials. This may thus provide a direct evidence of the covalent grafting of **2**. Indeed, these supplementary thiourea functions result necessarily from the reaction of the amine groups with the —NCS group brought by **2**, and cannot be due to the presence of unreacted POMs thanks to the use of efficient washing steps with soxhlet techniques.

Finally, **2**@{NH_2}—SBA-15 was also studied by ^{31}P CP-MAS NMR spectroscopy (Fig. 8). Demonstration for the retention of the integrity of POM entities upon grafting onto {NH_2}—SBA-15 was brought through the presence of a single large peak at −12.8 ppm, in accordance with the chemical shift of **2** observed in solution (see experimental part). No other phosphotungstate species were thus detected by this technique in the final hybrid material.

3.3. Evaluation of the catalytic performances of the anchored 2@{NH_2}—SBA-15 catalyst

The model reaction tested was the epoxidation of cyclooctene with aqueous H_2O_2. It was carried out at room temperature in acetonitrile with a catalyst:alkene:H_2O_2 ratio equal to 1:250:250. As expected, no reaction occurred in the absence of the catalysts and it was also verified that no H_2O_2 consumption was detected in the absence of cyclooctene. With cyclooctene, the expected selectivity is 100% with the epoxide as only product.

Prior to the study of the catalytic performances of **2** covalently supported onto mesoporous silica, we checked the activity of **1** and **2** under homogeneous conditions. The results of cyclooctene conversion are presented in Fig. 9. As indicated, the behavior of these two complexes was rather different. Compound **1** after 24 h led to a cyclooctene conversion of 97% *vs* 43% once the PDITC is grafted on the amine-functions of the POM (compound **2**). The decrease of the conversion could be due to the steric hindrance generated by the PDITC functions. However, the absence of free NH_2 groups, namely basic functions (at the difference of **1**) that could help the deprotonation of hydrogen peroxide or hydroperoxo ligands coordinated to tungsten (+VI) cations may also explain the catalytic decrease.

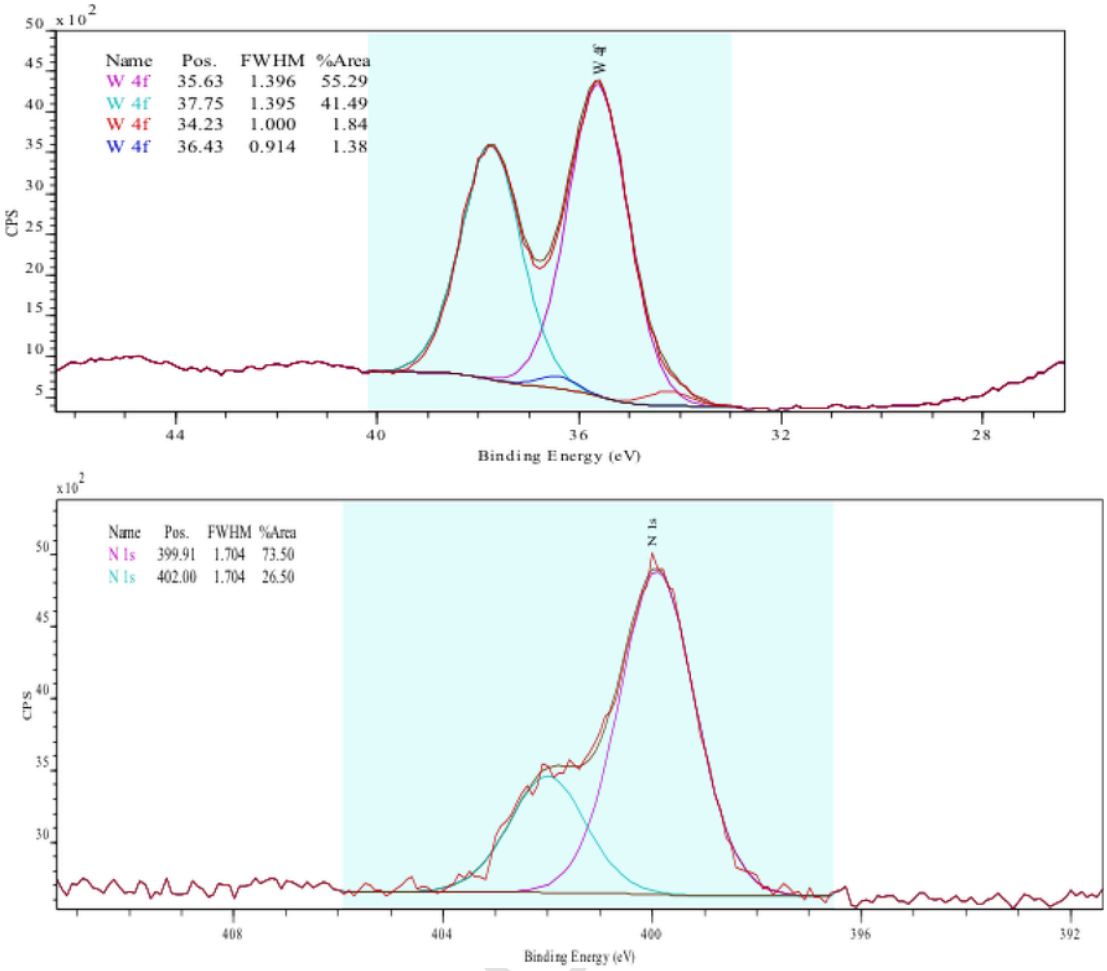

Fig. 6. High Resolution W_{4f} (top) and N_{1s} (bottom) XPS spectra of POM-PDITC immobilized onto amino-functionalized SBA-15.

In a second step, the supported **2**@{NH_2}—SBA-15 catalyst was used towards cyclooctene epoxidation in analogous conditions (same catalyst:alkene:H_2O_2 ratio, room temperature) as for its homogenous counterpart. Once compound **2** was grafted onto the surface of amino-functionalized SBA-15, the cyclooctene conversion decreased significantly (8%). This behavior is very similar to the results previously observed in our precedent work concerning the immobilization of compound **1** onto {COOH}—SBA-15 using a coupling agent (isobutylchloroformiate) [12]. In this former example, in the same conditions, we obtained a conversion of 19%, significantly lower than that of **1** in homogeneous conditions. However, in the present study, it is noteworthy that an increase of the temperature up to 50 °C (catalyst:alkene:H_2O_2 ratio equal to 1:250:250) for the supported **2**@{NH_2}—SBA-15 catalyst led to a catalytic efficiency (conversion of cyclooctene = 53%) higher than that of **2** at RT. It should be noted that the conversion of cyclooctene with compound **2** in homogeneous conditions was found equal to 100% at 50 °C, after 24 h.

4. Conclusion

In this work we described the preparation, the complete characterization and the catalytic behavior of a new supported hybrid of polyoxometalate catalyst. The immobilization of the catalyst in this study was obtained through a very simple strategy, adapted from grafting protocols used for biomolecules onto various {NH_2}-functionalized surfaces. The covalent grafting of **1** was successfully achieved in a facile two-step strategy using a cross-linker (PDITC) bearing two isothiocyanate functions. The reaction of PDITC with **1** thus allowed the bis-functionalization of the anion in a quantitative yield in mild conditions (room temperature) and without the production of co-products. In a second step, the post-functionalized hybrid of polyoxometalate **2** was reacted with the {NH_2}—SBA-15 support, leading to the formation of robust thiourea functions between **2** and the aminopropyl groups of the support. The formation of the covalent thiourea link was confirmed by ^{13}C CP-MAS NMR spectroscopy and the catalytic behavior of the grafted catalyst was then tested in a model reaction (epoxidation of cyclooctene). As in our previous reported work, the immobilization of the catalyst **2** led to a decrease of the catalytic performance, but slight modifications of the experimental conditions (a moderate increase of the temperature up to 50 °C) allowed a similar conversion of cyclooctene to that observed in homogeneous conditions at room temperature.

In conclusion, this study confirmed that organic/inorganic hybrid derivatives of POMs are a new class of catalysts that offer some great advantages in comparison with classical POMs and transition metal substituted POMs: due to the presence of useful organic functions, hybrids of POMs are thus able to covalently bind an inorganic support using different linking strategies. We have thus shown that their covalent immobilization came along with their excellent dispersion all along the channels of the SBA-15 support, a criterion that meets expectations of an efficient heterogenized catalyst. We also showed that the existence of a covalent link did not prevent the catalytic reactivity of these supported systems.

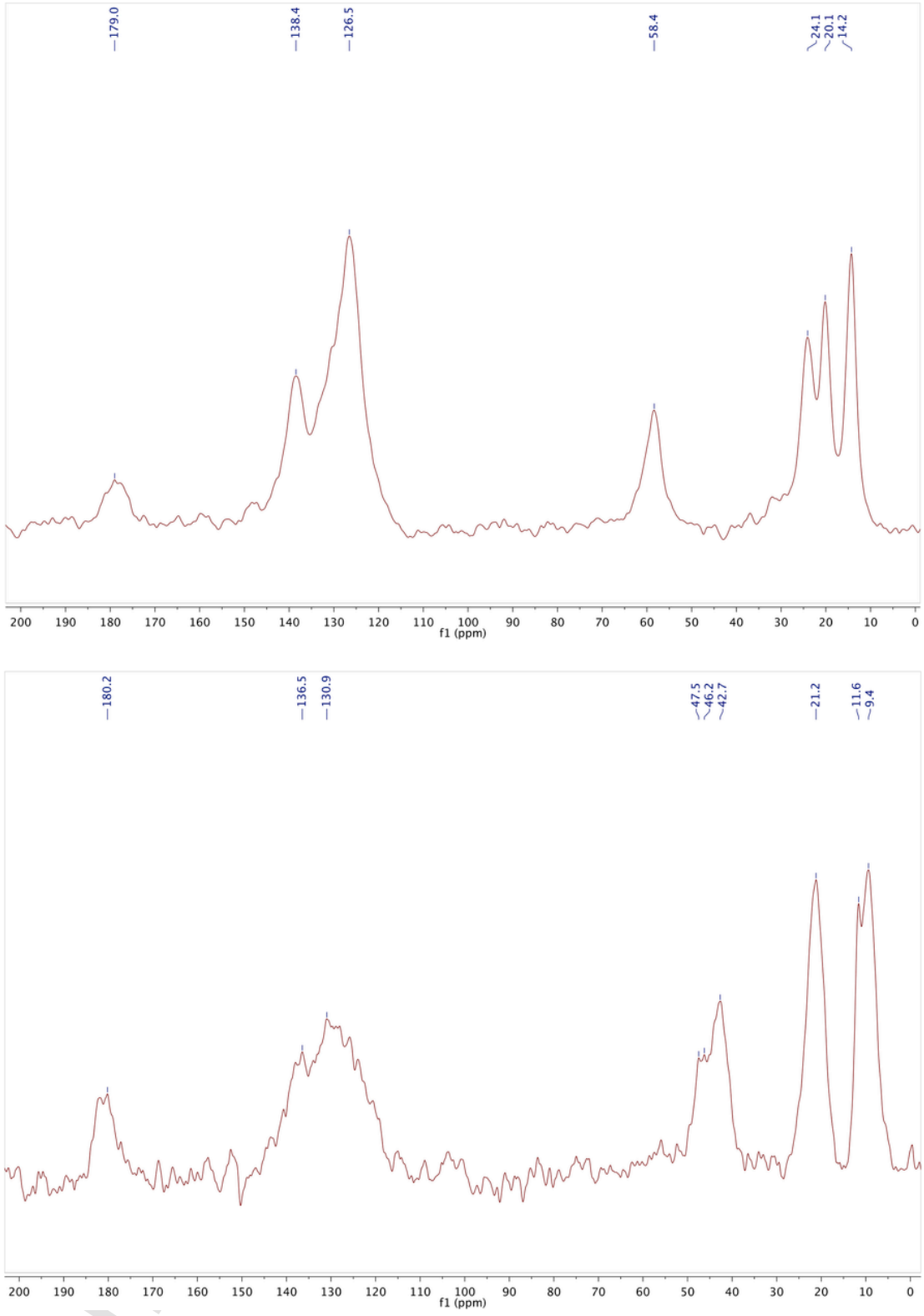

Fig. 7. ^{13}C CP-MAS NMR spectra of **2** (top) and of **2** immobilized onto amino functionalized SBA-15 (**2**@{NH_2}—SBA-15) (bottom).

Finally, and this is an important point of this work, we have shown that it was possible to control the grafting of a molecular catalyst using a cross-linker when this one is first linked to the molecule introduced and not first linked to the surface. The former strategy is barely used in the literature, since cross-linkers are generally introduced for function-

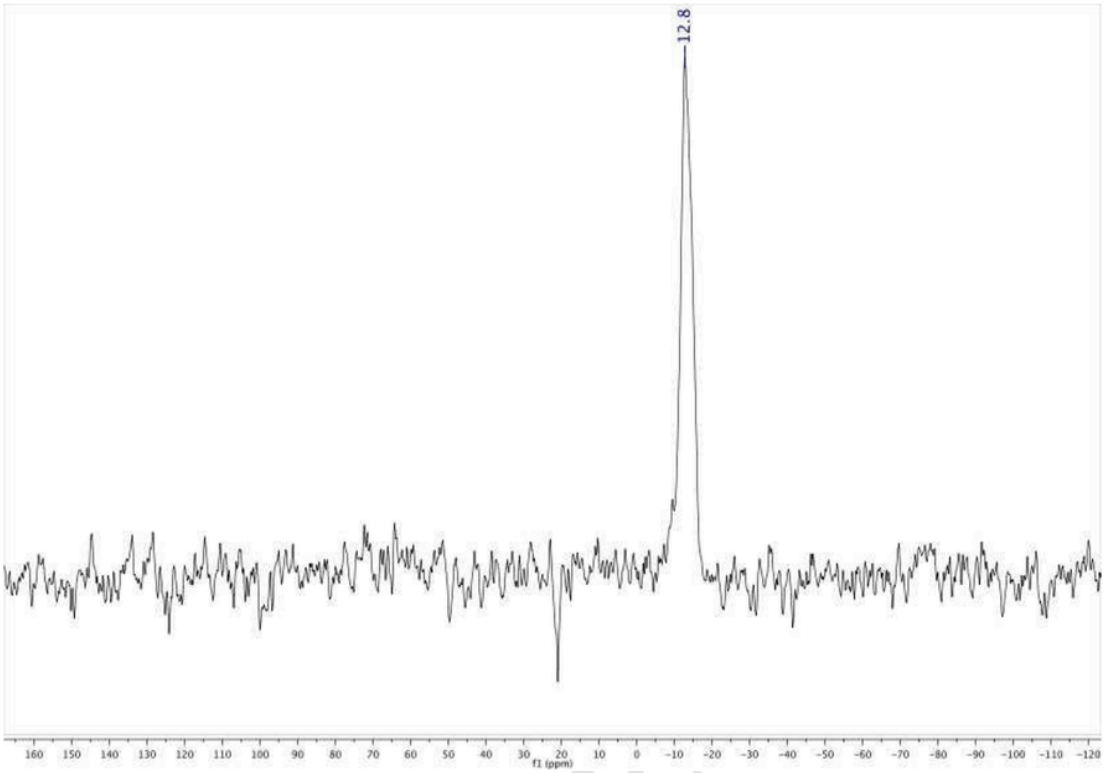

Fig. 8. ^{31}P CP-MAS NMR spectrum of **2** @{NH_2}—SBA-15.

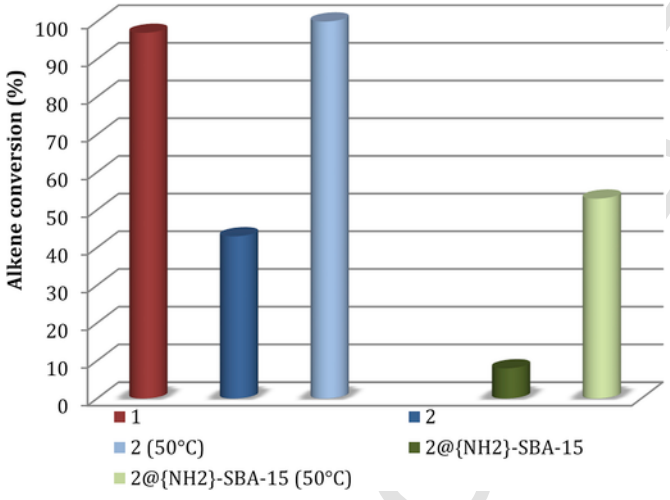

Fig. 9. Diagram for cyclooctene conversion (CH_3CN, after 24 h) i) in homogeneous conditions at room temperature with **1** (red), **2** (dark blue), and at 50 °C with **2** (light blue); ii) with supported catalysts **2**@{NH_2}—SBA-15 at room temperature (dark green) and at 50 °C (light green). (For interpretation of the references to colour in this figure legend, the reader is referred to the Web version of this article.)

alizing a surface in view of the recognition of a molecule of biological interest.

Appendix A. Supplementary data

Supplementary data to this article can be found online at https://doi.org/10.1016/j.micromeso.2018.11.036.

References

[1] N. Mizuno, K. Kamata, K. Yamaguchi, Top. Catal. 53 (2010) 876–893, Ed. C.L. Hill Special Issue on Polyoxometalates in Catalysis. J. Mol. Cat. A: Chem. 262 (2007) 1-242. I. V. Kozhevnikov, Catalysts for Fine Chemical Synthesis Vol. 2: Catalysis by Polyoxometalates (2002) Wiley, Eds: S. M Roberts, I. V Kozhevnikov, E. Derouane.

[2] D.E. Katsoulis, Chem. Rev. 98 (1998) 359–387, T. Okuhara, N. Mizuno, M. Misono, Appl. Catal., A 222 (2001) 63-77. Sustainable Heterogeneous Acid Catalysis by Heteropoly Acids. In Handbook of Green Chemistry, Vol. 2 Wiley-VCH: Weinheim, Eds: P. T.Anastas, R. H. Crabtree, (2009)153-174.

[3] T. Kimura, K. Kamata, N. Mizuno, Angew. Chem. Int. Ed. 51 (2012) 6700–6703, K. Sugahara, T. Kimura, K. Kamata, K. Yamaguchi, N. Mizuno, Chem. Commun. 48 (2012) 8422-8424.

[4] Z.Y. Wei, M.H. Dickman, M.T. Pope, Inorg. Chem. 36 (1997) 130–131, J.S. Yadav, B.S. Reddy, K. Purnima, K. Nagaiah, N. Lingaiah, J. Mol. Catal. A 285 (2008) 36-40.

[5] G.D.K. Kumar, S. Baskaran, Chem. Commun. (2004) 1026–1027.

[6] I. Boldini, G. Guillemot, A. Caselli, A. Proust, E. Gallo, Adv. Synth. Catal. 352 (2010) 2365–2370.

[7] N. Mizuno, K. Yamaguchi, K. Kamata, Coord. Chem. Rev. 249 (2005) 1944–1956, R. Neumann, Inorg. Chem. 49 (2010) 3594-3601. N. Mizuno, K. Kamata, Coord. Chem. Rev. 255 (2011) 2358-2370. K. Kamata, K. Yonehara, Y. Nakagawa, K. Uehara, N. Mizuno, Nature Chem. 2 (2010) 478-483.

[8] M.T. Pope, Heteropoly and Isopoly Oxometalates, Springer-Verlag, Berlin, 1983, Topical issue on Polyoxometalates: Chem. Rev. 98 (1998) 1-387. Polyoxometalates: From Synthesis to Industrial Applications Eds: M.T. Pope, A. Müller, Kluwer, Dordrecht, The Netherlands (2001).

[9] C.L. Hill, O.A. Kholdeeva, in: M.G. Clerici, O.A. Kholdeeva (Eds.), Liquid Phase Oxidation via Heterogeneous Catalysis: Organic Synthesis and Industrial Applications, Wiley, New Jersey, 2013, pp. 263–319, O. A. Kholdeeva, N. V. Maksimchuk, G. M. Maksimov, Catal. Today 157 (2010) 107-113.

[10] J.-M. Bregeault, J.-Y. Piquemal, E. Briot, E. Duprey, F. Launay, L. Salles, M. Vennat, A.-P. Legrand, Microporous Mesoporous Mater. 44–45 (2001) 409–417.

[11] A. Proust, B. Matt, R. Villanneau, G. Guillemot, P. Gouzerh, G. Izzet, Chem. Soc. Rev. 41 (2012) 7605–7622.

[12] F. Bentaleb, O. Makrygenni, D. Brouri, C. Coelho Diogo, A. Mehdi, A. Proust, F. Launay, R. Villanneau, Inorg. Chem. 54 (2015) 7607–7616.

[13] O. Makrygenni, E. Secret, A. Michel, D. Brouri, V. Dupuis, A. Proust, J.-M. Siaugue, R. Villanneau, J. Colloid Interface Sci. 514 (2018) 49–58.

[14] F. Rusmini, Z. Zhong, J. Feijen, Biomacromolecules 8 (2007) 1775–1789, P. Jonkheijm, D. Weinrich, H. Schröder, C. M. Niemeyer, H. Waldmann, Angew. Chem. Int. Ed. 47 (2008) 9618-9647.

[15] J. Spadavecchia, J. Moreau, J. Hottin, M. Canva, Sens. Actuators, B 143 (2009) 139–143.

[16] Z. Guo, R.A. Guilfoyle, A.J. Thiel, R. Wang, L.M. Smith, Nucleic Acids Res. 22 (1994) 5456–5465, T. Auletta, B. Dordi, A. Mulder, A. Sartori, S. Onclin, C. M. Bruinink, M. Peter, C.A. Nijhuis, H. Beijleveld, H. Schoenherr, G. J. Vancso, A. Casnati, R. Ungaro, B.J. Ravoo, J. Huskens, D.N. Reinhoudt, Angew. Chem. Int. Ed. 43 (2004) 369-373.
[17] R. Benters, C.M. Niemeyer, D. Drutschmann, D. Blohm, D. Wöhrle, Nucleic Acids Res. 30 (2002) E10.
[18] N. Aissaoui, L. Bergaoui, S. Boujday, J.-F. Lambert, C. Methivier, J. Landoulsi, Langmuir 30 (2014) 4066–4077.
[19] X. Zeng, Y. Xu, X. Chen, W. Ma, Y. Zhou, Appl. Surf. Sci. 423 (2017) 1103–1110, H. Huang, F. Dong, Y. Tian, Anal. Chem. 88 (2016) 12294-12302.
[20] M.I. Kim, H.O. Ham, S.-D. Oh, H.G. Park, H.N. Chang, S.-H. Choi, J. Mol. Catal. B Enzym. 39 (2006) 62–68, Y. Zhu, Y. Fang, L. Borchardt, S. Kaskel, Stefan Microporous Mesoporous Mater. 141 (2011) 199-206. D. Angelova, L. Armelao, S. Gross, G. Kickelbick, R. Seraglia, E. Tondello, G. Trimmel, A. Venzo, Appl. Surf. Sci. 226 (2004) 144-148.
[21] E.E. Bedford, S. Boujday, V. Humblort, F.X. Gu, C.-M. Pradier, Colloids Surf., B 116 (2014) 489–496.
[22] H.J. Kim, S.J. Lee, S.Y. Park, J.H. Jung, J.S. Kim, Adv. Mater. 20 (2008) 3229–3234.
[23] R. Villanneau, A. Ben Djamâa, L.-M. Chamoreau, G. Gontard, A. Proust, Eur. J. Inorg. Chem. (2013) 1815–1820.
[24] M. Boutros, G. Shirley, T. Onfroy, F. Launay, Appl. Catal., A 394 (2011) 158–165.
[25] R. Villanneau, A. Marzouk, Y. Wang, A. Ben Djamaa, G. Laugel, A. Proust, F. Launay, Inorg. Chem. 52 (2013) 2958–2965.
[26] D. Mercier, S. Boujday, C. Annabi, R. Villanneau, C.-M. Pradier, A. Proust, J. Phys. Chem. C 116 (2012) 13217–13224.
[27] R. Villanneau, A. Roucoux, P. Beaunier, D. Brouri, A. Proust, RSC Adv. 4 (2014) 26491–26498.
[28] D. Cauzzi, M. Lanfranchi, G. Marzolini, G. Predieri, A. Tiripicchio, M. Costa, R. Zanoni, J. Organomet. Chem. 488 (1995) 115–125.
[29] L.V. Sudha, D.N. Sathyanarayana, S. Narasimha Bharati, Magn. Reson. Chem. 25 (1987) 474–479.